ELSEVIER

A Three-Phase Model of the Elastic and Shrinkage Properties of Mortar

C.M. Neubauer,* H.M. Jennings,*† and E.J. Garboczi‡
*Department of Materials Science and Engineering and †Department of Civil Engineering, Northwestern University, Evanston, Illinois, and ‡National Institute of Standards and Technology, Building Materials Division, Gaithersburg, Maryland

Mortar and concrete are composite materials with overall properties that are influenced by the arrangement and characteristics of each constituent in the microstructure. Elastic shrinkage, like other properties of mortar and concrete, must be described by a three-phase model: aggregate, bulk cement paste, and interfacial transition zone (ITZ) cement paste. A simple two-dimensional digital-image-based model of a mortar is developed based on the hard core/soft shell percolation model. Specific attention is given to the properties of the ITZ between cement paste and aggregate. The elastic shrinkage properties of this model are computed numerically, using a specialized finite-element technique. The effects of varying the elastic moduli and shrinkage properties of the ITZ and bulk cement paste are examined in parameter studies, both analytically, for low aggregate content, and numerically, for arbitrary aggregate content. Special attention is given to the effect that the topology of the ITZ has on overall shrinkage. A comparison is made between model predictions and the limited available experimental results (0.35 w/c, 65% hydration), assuming an ITZ width of 20 μm. Based on this comparison, this paper introduces the prediction that the Young's modulus of the ITZ is one third to one half of the modulus for bulk cement paste and that the unrestrained shrinkage of the ITZ material is close to the shrinkage of bulk cement paste when both are averaged over a 20-μm ITZ. This finding is supported by further analysis of a three-dimensional microstructural model of cement paste. ADVANCED CEMENT BASED MATERIALS 1996, 4, 6–20

KEY WORDS: Cement, Concrete, Drying shrinkage, Elastic properties, Finite element, Interfacial transition zone, Mortars

The drying shrinkage of mortar and concrete, as with almost any other physical property of these materials, depends on the microstructure over a wide range of length scales [1,2]. The shrinkage of the C-S-H (C = CaO, S = SiO_2, H = H_2O) gel, which controls the shrinkage of cement-based materials, is determined, at the most fundamental level, by the rearrangement of water in the nanometer-scale gel pores as relative humidity is reduced. Cement paste is a complex composite at the micrometer length scale, being a mixture of a phase that shrinks under drying (C-S-H) and restraining phases that have negligible shrinkage upon drying, like unreacted cement and calcium hydroxide (CH). In portland cement paste, there are aluminate, ferrite, and sulfate phases that can also act as restraining phases. The analysis in this paper is general, but where we consider cement paste microstructure and properties directly, we only consider C_3S cement paste for simplicity. Mortar and concrete are also complex random composites, but at the millimeter to meter length scale. Because they are composed of both nonshrinking aggregate and shrinking cement paste, their overall shrinkage response depends on the relative amounts of these phases and their arrangement in the microstructure.

Models have already been developed to simulate the movement of water in structural models of C-S-H and porous Vycor at the nanometer scale [3,4]. At this level, a model must account for solid, liquid, and air phases. In addition, shrinkage stresses, generated by surface forces, must be modeled at the solid/liquid, liquid/air, and solid/air interfaces. For this paper's analysis, the material is treated as a composite at a larger length scale where each phase is a continuum material with specified properties. For shrinkage, each phase is given a set of elastic moduli and an unrestrained shrinkage parameter. The unrestrained shrinkage (sometimes referred to as the "eigenstrain" of a phase [5]) is the shrinkage strain that would occur in an isolated, unrestrained condition. This description makes use of the analogy between length changes due to temperature changes and length changes that occur under humidity changes [6].

This paper reports the results of modeling mortars using digital-image models, where each pixel is 10 μm across. Mortar is known to be a three-phase composite: aggregate, bulk cement paste, and interfacial transition zone (ITZ) cement paste. The ITZ is modeled as a phase with a single property, rather than a gradient of properties, which admittedly is a simplification. Each phase is given appropriate elastic moduli and unrestrained

Address correspondence to: Hamlin M. Jennings, Department of Civil Engineering, Northwestern University, 2145 Sheridan Road, Evanston, IL 60208.
Received April 17, 1995; Accepted January 16, 1996

ISSN 1065-7355/96/$15.00
PII S1065-7355(96)00024-7

shrinkage strains. These models are two-dimensional because of present computer-imposed resolution limitations in three dimensions. In two dimensions, large enough arrays (number of pixels per unit length) can be generated to adequately resolve the interfacial zone region and to represent a statistically meaningful number of sand grains. Carrying out this kind of computation in three dimensions will be dependent on computer memory and speed developments in the next few years, although the high-end of present-day supercomputers is very close to being able to run 512^3 finite element simulations. This would give resolution comparable to the present two-dimensional (2-D) simulations. As a result of the restriction to two dimensions, qualitative insight into existing experimental results is sought, rather than quantitative agreement.

It is important to note that only elastic, reversible shrinkage is computed, which is another limitation of the model at present. It is, of course, well known that the shrinkage of cement-based materials has a strong irreversible component and contributions from creep [1]. However, a model predicting this type of behavior for arbitrary microstructures is currently unavailable and would be extremely computer-intensive if it did exist. Thus, it seems logical to fully explore the simpler case of elastic shrinkage before moving on to more complicated models. There is general agreement in the scientific community that ITZ properties do affect overall moduli and shrinkage. This paper represents the beginning of an attempt to show how the ITZ affects these properties.

Section I describes the details of the models themselves. Section II discusses the effect on the elastic moduli of mortar by varying the ITZ and bulk cement paste moduli. Section III describes differences in unrestrained shrinkage and moduli between the ITZ and bulk cement paste and how this affects shrinkage of mortar. Also, an exact analytical equation is introduced and used to analyze real experimental shrinkage data for the shrinkage of mortars containing small concentrations of sand. Section IV describes computational results for cement paste shrinkage at the micrometer scale. These results help explain the relationship of shrinkages in the ITZ to shrinkages in the bulk cement paste found in the previous section. Section V summarizes the results of this work.

I. Models for Elastic Properties and Microstructure

The numerical algorithm utilized in the model to determine elastic moduli and shrinkage has previously been described [7]. It uses a linear finite element code to operate on a two-dimensional digital image of a random, multiphase composite. Each pixel is treated as a simple bilinear finite element, with displacements defined at the pixel corners. The moduli of each pixel are defined by its phase label. The finite element mesh is then simply defined by the digital image. Digital images of arbitrary microstructures can be analyzed, such as those of portland cement paste [8].

Two different computations can be performed. First, the effective moduli of a composite system can be computed by applying an overall strain to the system. The algorithm uses a modified conjugate gradient solver to determine the set of nodal displacements, which minimizes the overall energy of the system, subject to the constraints of the applied strain. The elastic stresses and strains in each pixel can be computed from the displacements.

To compute the shrinkage, we allow the size of the system, in addition to the nodal displacements, to vary. Each phase has a certain unrestrained shrinkage that competes with the rigidity of the rest of the system to produce an overall shrinkage. When the energy is minimized, the average stress is zero, but the individual stresses in each pixel are generally non-zero. The new size of the sample then gives the composite, or overall, shrinkage value.

Because the algorithm models two-dimensional space, it is necessary to decide how to map three dimensional (3-D) elastic properties into a 2-D medium by choosing either a plane stress or a plane strain criterion. Plane stress is appropriate [9], assuming that the two-dimensional digital images represent thin sheets of 3-D material. In such a situation, the Young's modulus, Poisson's ratio, and shear modulus are unchanged between three and two dimensions. The 2-D bulk modulus, K_2, is calculated as:

$$K_2 = \frac{9K_3G_3}{3K_3 + 4G_3} \tag{1}$$

where K_3 and G_3 are the bulk and shear moduli in three dimensions. The assumption of plane strain or stress does not actually make a significant qualitative difference in the overall computed behavior.

Another important assumption is used with regard to the width of the ITZ in the model. The ITZ is usually described as a region 30–50 μm in thickness [10] in which the cement paste composition differs significantly from that of the bulk cement paste. This region typically displays much higher porosity and CH volume fractions, and lower C-S-H gel and unhydrated cement volume fractions [11], than in the bulk cement paste. This is attributed, in part, to reduced efficiency in particle packing near the surface of the aggregate particle [10,11].

In the computations described in this paper, the ITZ

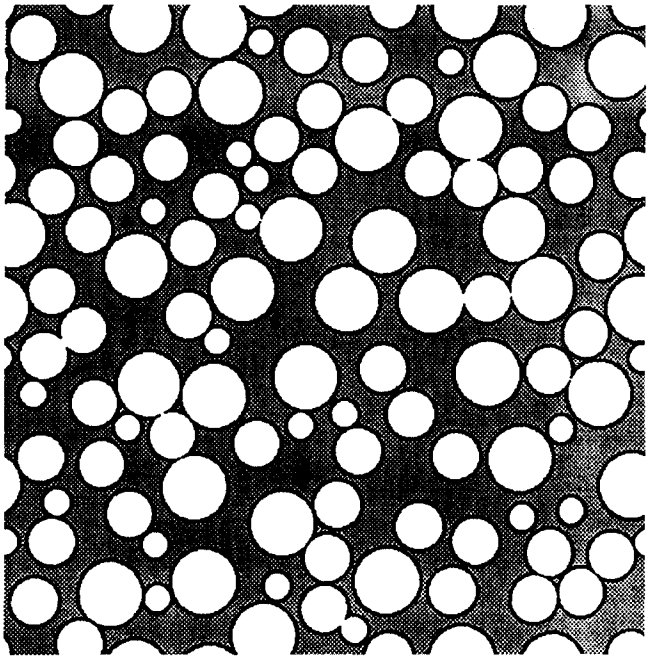

FIGURE 1. Digital image of mortar using sand distribution in Table 1 (white = sand; grey = bulk cement paste, black = interfacial transition zone cement paste).

is assumed to have a width of approximately $h = 20$ μm [12]. The properties and composition of the zone are considered to be constant across this 20-μm width and represent the average properties of the entire zone region. This simplification is necessary because of the difficulties in simulating the effective properties of a region when properties and composition change rapidly over small length scales. To simulate the overall arrangement of sand grains and interfacial zone areas, the hard core/soft shell model, previously used for 3-D simulation of mortar microstructures, is used [12]. Composite grains, consisting of a circular hard core (sand), surrounded by a concentric circular soft shell (interfacial zone cement paste), are deposited randomly in a matrix (bulk cement paste). The hard cores may not be overlapped, but the soft shells may overlap each other or the bulk cement paste phase. Figure 1 shows a typical 2-D mortar microstructure generated with this

TABLE 1. Ottawa sand distribution for simulation of Pickett data taking 1 pixel = 10 μm

Diameter (μm)	Sieve Size	Number Percent of Distribution
510	#30–40	30
370	#40–50	50
210	#50–100	20

TABLE 2. Comparison of interfacial transition zone (ITZ) volume per particle

Diameter (μm)	$\text{Volume}_{ITZ}/\text{Volume}_{particle}$ (3-D)	$\text{Area}_{ITZ}/\text{Area}_{particle}$(2-D)
110	1.536	0.860
210	0.687	0.417
310	0.439	0.275
410	0.322	0.205
510	0.254	0.163
910	0.138	0.090

algorithm, using the size distribution of sand grains given in Table 1. No attempt has been made to determine the 2-D sand size representations by taking slices of a real 3-D sand size distribution, as has been done in other works [13]. The distributions are only 2-D but are suitable for qualitative insight.

There are obviously other differences between two and three dimensions. In three dimensions there is a much higher volume percentage of ITZ per particle than in two dimensions, as shown in Table 2 for isolated particles. This is a geometrical fact and is easily illustrated. If the interfacial transition thickness $h << r$, the particle radius, then in two dimensions this ratio is $2h/r$, and in three dimensions it is $3h/r$. The ratio of these two ratios would then be 3/2. In Table 2, it can be seen that the ratio of ratios is above 3/2 but is decreasing continuously towards this value as r increases at a fixed value of h. It has been found that the actual volume of interfacial zone cement paste in realistic 3-D models is within 5% of that calculated by simply multiplying the sand surface area by h, the ITZ thickness [12]. This implies that the ratio of ITZ volume to particle volume is nearly the same as for a single particle. This result has been seen to be valid for sand volume fractions as high as 50%. The same effect occurs in two dimensions, as will be discussed in the next section. This results in a higher percentage of ITZ cement paste in the 3-D mortar than in the 2-D mortar with the same sand content. In addition, in two dimensions there is usually more overlap of the ITZs, which also results in an effectively lower area of ITZ at a given sand area fraction.

Percolation of the ITZs is another important factor. The 2-D models in this paper mostly did not have percolated ITZs, inconsistent with 3-D models [12]. However, overall shrinkage should be relatively unchanged, as the elastic properties of the ITZ and bulk cement paste are within a factor of 2 or 3. This is not a large difference in terms of percolation effects [14].

To test the accuracy of the elastic algorithm, a series of computations was performed on a set of mortar images. The properties of the shells (interfacial zone cement paste) were taken to be identical to the matrix (bulk cement paste) in order to reduce the number of elastically different phases from three to two. Each mi-

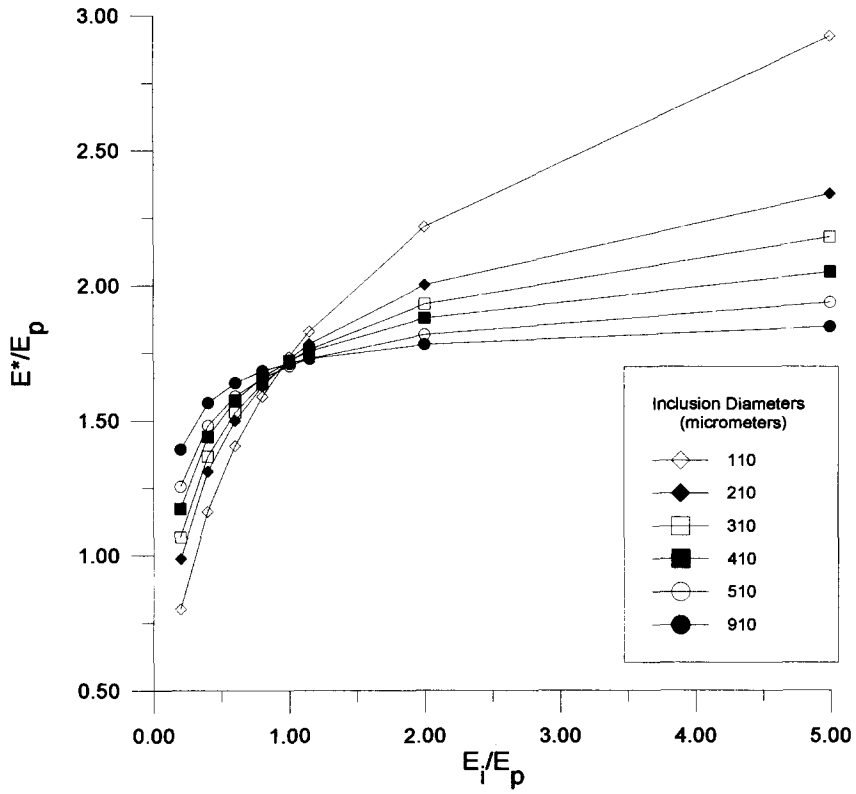

FIGURE 2. Effect of the ratio of the interfacial transition zone cement paste Young's modulus, E_i, to the bulk cement paste Young's modulus, E_p, on the composite Young's modulus, E^*, for different sand particle diameters at a constant area fraction of 55%.

crostructure was created using monosized circular sand grains of diameters 110, 210, 310, 410, and 510 μm in a 5.12 × 5.12-mm image. For each particle size, a range of sand area fractions was used, from 10% to 55%. The Young's modulus of the sand grains was set to three times the bulk cement paste matrix. The Poisson's ratios of the bulk cement paste and sand grains were set to 0.3 and 0.2, respectively. These values were derived from elastic moduli values [15] and are reasonable choices for mortars, as will be discussed later. For shrinkage analysis, the sand phase was assumed to be nonshrinking, while the bulk cement paste was given an arbitrary shrinkage. Exact values for the bulk cement paste Young's modulus and unrestrained shrinkage are not important in these 2-D composites since all results are normalized by these values. All values of the effective elastic moduli and shrinkage strains agreed well with previous numerical and analytical results [16–18]. In particular, the Hashin-Rosen [19] exact prediction for shrinkage in terms of the effective bulk modulus for a two-phase system agreed very closely with the numerical tests. For the two-phase test, the effective elastic moduli were independent of the sand size used, which was expected for monosize circular inclusions.

II. ITZ Effects on the Elastic Moduli of Mortars

The influence of the ITZ on the elastic properties and shrinkage of mortars has recently begun to be addressed [20,21]. The quantitative effect of this third phase is dependent upon its inherent properties and location within the microstructure. The location of the ITZ is handled well by the present model, but three unknowns for the interfacial region must still be quantified: two elastic moduli and the unrestrained shrinkage strain of the ITZ. The elastic moduli are considered in this section.

To explore the effect of the ITZ, models were created using monosize circles for sand grains, where the surface area of the sand grains, at a constant area fraction of 55%, was adjusted by using different diameters (110–910 μm) in order to compare with recent experimental results using similar systems [22]. A 20-μm-thick interfacial zone surrounded each of the sand particles. The Young's moduli and Poisson's ratios from Section I were used for sand (E_s) and bulk cement paste (E_p), while the Poisson's ratio of the interface was set to 0.3 (the same as the paste) and the Young's modulus of the

interface (E_i) was varied from 20% to 500% of the paste ($0.2 < E_i/E_p < 5$). Due to the usually higher porosity of the ITZ paste in real mortars and concrete, the Young's modulus of the interfacial region is expected to be lower than the Young's modulus of the bulk. Helmuth and Turk [23] described their experimentally obtained moduli for a wide range of cement pastes and degrees of hydration by the expression:

$$E = E_{gel}(1 - V_c)^3 \quad (2)$$

where E is the overall modulus of the paste, E_{gel} is the average modulus of the hydration products, and V_c is the capillary porosity. However, in the model, E_i/E_p was allowed to be greater than one, because we wish to see the full range of behavior and because, for lightweight aggregates and chemically treated aggregates, $E_i/E_p > 1$ could be physically realistic [24].

Figure 2 shows the results of these numerical experiments, with E^*/E_p plotted against E_i/E_p, where E^* is the overall composite modulus. Two distinct regions are apparent. As expected, at points where the interface moduli are less than the paste, the modulus of the composite material is decreased by the presence of the interfacial zone. Similarly, when the modulus of the interface is stiffer than the paste matrix, the modulus of the overall composite is increased. The magnitude of the increase or decrease varies significantly with the diameter of the aggregate particle, due to the varying amounts of interfacial zone phase present. As this diameter increases, there is less interfacial zone area per unit area of inclusion for isolated sand grains and sand grains at area concentration of 55%, as shown in Table 3. More importantly, as can be seen in the last column of Table 3, the mortars with higher surface area sand have a larger area fraction of interfacial zone, and so the moduli of this phase have a correspondingly larger effect on the overall composite moduli. Also in Table 3, it can be seen that for particles larger than 210 μm, the area of the ITZ per particle area is only slightly smaller for the 55% sand systems than for isolated particles, implying that indeed the overlap area is small, even at this fairly high sand area fraction. However, for the 110 and 210 μm diameter sand grains, since $h = 20$ μm is a large fraction of the sand grain diameter, there is a fairly large amount of ITZ overlap, as can be seen in the differences between the second and third columns in Table 3.

Separating the two regions of Figure 2 is a point where the interface moduli are equal to the bulk paste moduli. At this point, the interface has elastic properties equal to the bulk paste and "disappears," in effect acting as simply more bulk paste. The moduli of all particle size composites converge to this point, as was discussed in Section I.

TABLE 3. Particle and interfacial transition zone (ITZ) areas for different size sand particles ($h = 20$ μm)

Diameter (μm)	$\text{Area}_{ITZ}/\text{Area}_{particle}$	$\text{Area}_{ITZ}/\text{Area}_{particle}$ (55% Sand)	Area Fraction of ITZ (55% Sand)
110	0.860	0.562	0.309
210	0.417	0.338	0.186
310	0.275	0.267	0.146
410	0.205	0.198	0.109
510	0.163	0.150	0.082
910	0.090	0.088	0.048

Based on existing experimental measurements [22], the E/E_p data from Figure 2 for $E_i/E_p < 1$ was replotted versus surface area of sand in Figure 3. An easily derived relation between surface area and the particle diameter for d-dimensional spheres was used:

$$SA = \frac{k}{\rho * d_{mean}} \quad (3)$$

where k is a constant given by $k = 2d$ (d is the number of dimensions), SA is the surface area in m^{d-1}/kg, ρ is the density of the aggregate (taken to be 2.56 g/cm^3, the value for quartzite, as in [22]), and d_{mean} is the mean diameter of the inclusion particles in meters. The 3-D value of $k = 6$ was used in order to relate more closely to the experimental results in the work of Cohen et al. [22], but, most significantly, the surface area and mean diameter are inversely related via eq 3. The actual value of the constant of proportionality is not important in this work.

Figure 3 clearly shows the effects of increasing the area fraction of interfacial zone by increasing the surface area of the sand. Each curve has a different value of E_i/E_p. Figure 3 is an important graph because, in principle, it allows for the quantification of E_i by comparison with experimental data in one of two ways, both of which require knowledge of the surface area of the aggregate and the moduli of the composite material.

The first method also requires knowledge of the moduli for the paste alone. A direct comparison can then be made by normalizing the measured composite moduli with the paste moduli, using the proper surface area, and then finding the best fitting E_i/E_p ratio from the graph.

In the second method, one would determine the experimental drop in E_i/E_p (percentage) as the surface area of the mortar aggregate is increased, assuming E_p

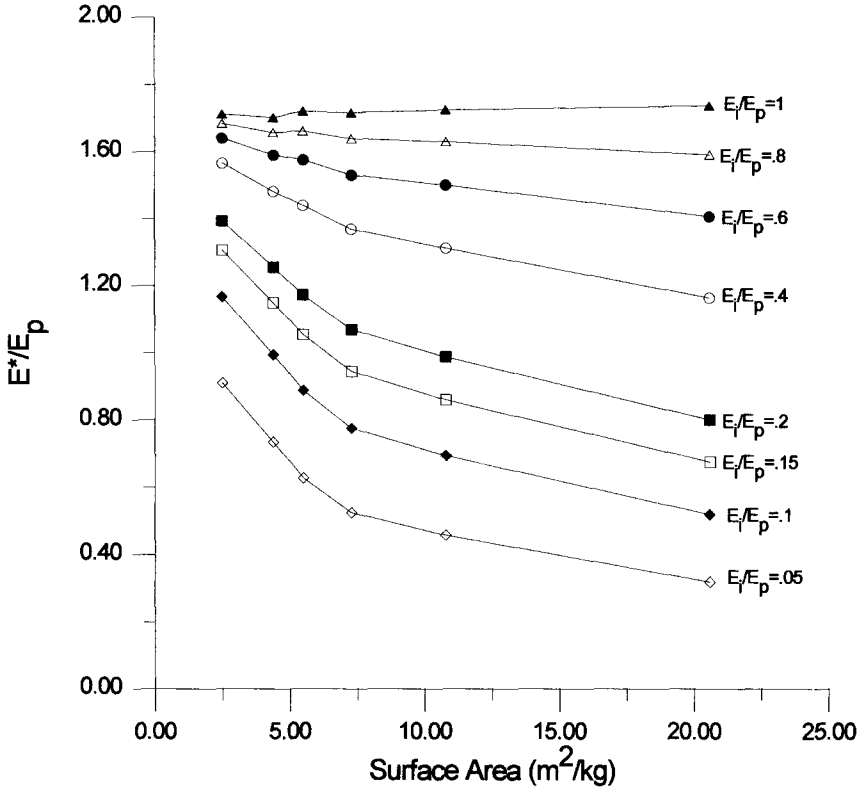

FIGURE 3. Effect of aggregate surface area on composite Young's modulus with changing interfacial/paste Young's modulus ratio for $E_i/E_p < 1$ for different sand particle diameters at a constant area fraction of 55%.

is a constant. This can then be compared to the percentage drops predicted by the algorithm for the various E_i/E_p ratios. The point at which theory and experiment agree determines the correct ratio.

The results of Figure 3 are from a 2-D model and so cannot be rigorously used in either of these methods to analyze 3-D experimental data. Furthermore, as sand surface area increases, ITZ area fraction also increases. Because of the higher porosity of the ITZ, it will have a higher water/cement ratio (w/c). Since the overall paste has a fixed w/c, conservation of water between bulk and ITZ implies that the bulk cement paste will increase in density by decreasing in w/c as the ITZ area fraction increases. Thus, strictly speaking, the moduli of the paste from which the mortar is made are not exactly the moduli to be used for the bulk paste in the mortar microstructure. However, such a comparison does provide some qualitative insight.

The elastic moduli of mortars as a function of surface area of sand for nearly monosize sand grains have been measured by Cohen et al. [22]. In their work, the dynamic elastic moduli of portland cement and silica fume mortars were measured as a function of surface area and of hydration time. In the present work, only their 28-day portland cement mortar data has been considered. Since the E_p for their data is unknown, the second method described previously was used.

In the data of Cohen et al., a Young's modulus of 33 GPa was measured for a mortar containing sand with surface area of 2.5 m^2/kg, and a Young's modulus of 29 GPa was measured for a mortar containing a sand surface area of 10 m^2/kg, representing a drop of 11.6% in modulus as the sand surface area was increased by a factor of 4. Using Figure 3, these values were bracketed between the curves of $E_i/E_p = 0.4$ (which had a drop of 16.2%) and $E_i/E_p = 0.6$, (which had a drop of 8.7%). It was found that $E_i/E_p \approx 0.5$ fit the experimental data reasonably well. This implies that, when averaging over an interfacial zone thickness of 20 μm, the effective Young's modulus of this region will be approximately one half that of the bulk cement paste, at least for fairly large degrees of hydration. This is a reasonable value, considering the higher porosity of the interfacial zone [25]. Also, this value can be checked through the use of eq 3. By taking an approximate value of 35% porosity at the interface and 7% in the bulk, as reported by Scrivener [10], for a 28-day-old concrete specimen of w/c = 0.5 [26], averaging the porosity over the interfacial region, and using eq 2 for both the interfacial region and the bulk, a modulus ratio of $E_i/E_p = 0.6$ is computed.

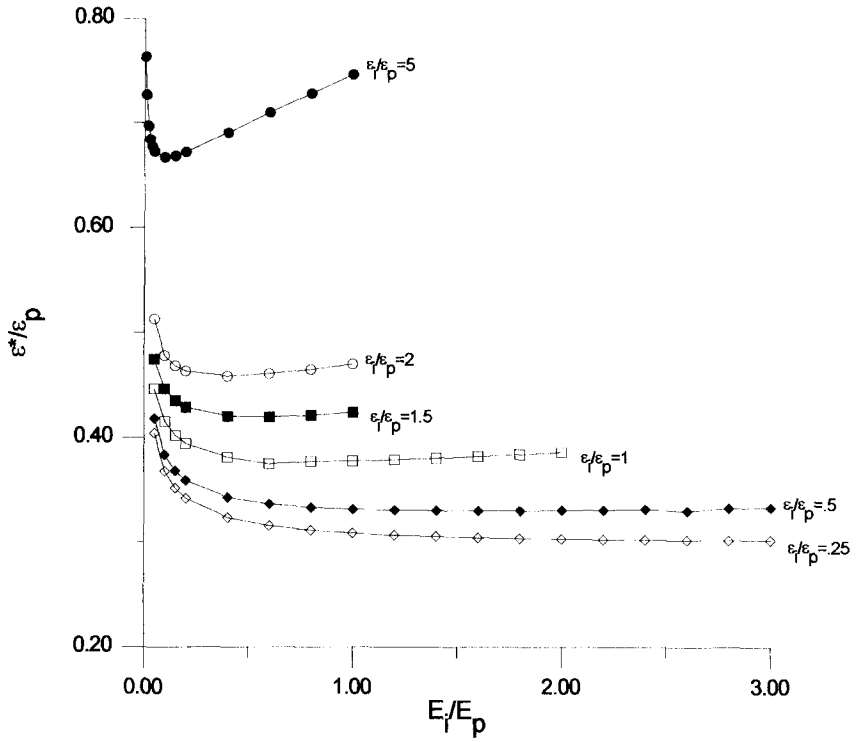

FIGURE 4. Effect of interfacial/paste Young's modulus ratio on composite shrinkage with changing interfacial shrinkage for a sand particle diameter of 410 μm at a constant area fraction of 55%.

This value is only a rough approximation, but it is in accord with the value fitted from the data of Cohen et al. [22]. Doing the same fitting procedure with a 3-D model would, of course, give a somewhat different answer.

III. Effects of ITZ on Shrinkage of Mortars

A. Numerical Results

Computations of shrinkage were performed on model microstructures with a 55% sand area fraction, in which each sand grain had a diameter of 410 μm and an interfacial zone thickness of 20 μm. These values were chosen to simulate a typical mortar, with 410 μm being a compromise between the number and mass weighted average diameters based on typical sand-size distributions [14]. The unrestrained shrinkage of the interfacial zone (ε_i) was allowed to vary from 25% to 500% of the paste shrinkage (ε_p), and the interfacial Young's modulus was varied so that $0.05 < E_i/E_p < 3$. Again, values of $E_i/E_p > 1$ are included for the cases of lightweight and chemically treated aggregates.

Figure 4 shows the results for $\varepsilon^*/\varepsilon_p$, as a function of E_i/E_p for different values of $\varepsilon_i/\varepsilon_p$, where ϵ^* is the overall composite shrinkage. The shape of the curves is interesting; for a given intrinsic strain ratio, $\varepsilon_i/\varepsilon_p$, there is a modulus ratio, E_i/E_p, which will minimize the shrinkage of the sample. This can be physically explained as follows.

At very low interfacial zone moduli, the overall shrinkage increases sharply as E_i/E_p decreases for any value of $\varepsilon_i/\varepsilon_p$. In this limit, the very soft interfacial zone essentially decouples the restraining aggregate from the shrinking bulk cement paste phase. The bulk paste no longer "sees" the nonshrinking aggregate and is able to shrink towards its intrinsic value; thus, $\varepsilon^*/\varepsilon_p$ tends toward 1. As the modulus of the interfacial zone increases, the bulk cement paste becomes more strongly coupled to the nonshrinking sand, decreasing the overall shrinkage. However, past a certain point, the increasing moduli of the interfacial zone cement paste causes the interface to act as a shrinking phase, which is well coupled to the bulk paste. The total paste phase can now better resist the restraining effect of the sand, thereby increasing the overall shrinkage and placing the aggregate in compression. The combination of these two mechanisms depends on the fact that, topologically, the bulk cement paste is physically separated from the sand by the interfacial zone phase. This topological fact is true in both two and three dimensions and is the cause of the observed minima in the curves in Figure 4. For lower values of $\varepsilon_i/\varepsilon_p$, the rise in $\varepsilon^*/\varepsilon_p$ with

TABLE 4. Average compressive stress in sand particles at E_i/E_p below, at, and above shrinkage minimums shown in Figure 4

$\varepsilon_i/\varepsilon_p$	Relation to Minimum	E_i/E_p	Shrinkage	Compressive Stress in Sand (Arbitrary Units)
	Below	1	-0.3321	0.259
0.5	At	2.6	-0.3316	0.327
	Above	3	-0.3366	0.341
	Below	0.1	-0.4167	0.157
1	At	0.6	-0.3788	0.253
	Above	2	-0.3871	0.378
	Below	0.02	-0.7044	0.072
5	At	0.05	-0.6789	0.110
	Above	0.5	-0.7050	0.361

increasing E_i/E_p is very shallow but is still numerically present.

The preceding analysis is confirmed in Table 4 by examining the average compressive stress per unit area of sand below, at, and above the minimum shown in Figure 4. As can be seen, the lowest compressive stress occurs when the paste is debonded from the sand particle at very low interfacial zone stiffness, indicating little interaction between the paste and sand. As the minimum is approached, the compressive stress per sand pixel increases, indicating that the sand particle is under compression as the bulk paste begins to exert more influence on the sand particle. Above the minimum, the compressive stress in the sand continues to increase as the interfacial zone begins to exert its own intrinsic shrinkage upon the particle, simultaneously increasing both the compressive stress and the overall shrinkage.

This result implies that to minimize the shrinkage of mortar and concrete, it may not necessarily be desirable significantly to stiffen the ITZ. The result is in direct contrast to strength considerations, where it is generally desirable to strengthen (and usually simultaneously stiffen) the ITZ as much as possible.

If knowledge of the shrinkage of the mortar specimen and its paste phase were known, the unrestrained shrinkage of the interfacial zone could be determined by comparing a 3-D version of Figure 4 to experimental data. Having determined the elastic modulus of the interfacial zone by one of the methods described in this section, the normalized shrinkage ratio in Figure 4 could be compared to determine the unrestrained shrinkage that best fits the experimental data.

An additional consideration is that real mortars and concretes almost always contain air voids. When air voids are introduced, the amount of the shrinking phase (cement paste) is reduced, but no restraint is added since the moduli of the air pore are taken to be zero. In effect, the average elastic moduli of the cement paste are reduced because the porosity of the nonsand matrix is increased. To explore this effect, two series of seven simulated model mortars were created with sand area fractions ranging from 5% to 55%. In one series, 4% (by total area) air was added, replacing an equivalent amount of cement paste. The sand grains had a diameter of 510 μm, and the air voids had a diameter of 110 μm. An interfacial zone of 20 μm was assigned to both [27]. The elastic properties and unrestrained shrinkage strains of the bulk paste, interfacial paste, and aggregate were: $E_p = 1.0$, $E_i = 0.5$, $E_a = 4.29$; $\nu_p = \nu_i = 0.3$, $\nu_a = 0.2$; $\varepsilon_p/\varepsilon_i < 0$, and $\varepsilon_a = 0$. The air voids were assumed to be empty, nonshrinking ($\varepsilon_v = 0$), and nonrestraining ($E_v = 0$), as noted above. For simplicity, the air voids were assumed to have no ITZ.

The results of these simulations are shown in Figure 5. Clearly, the presence of the air voids will decrease the magnitude of shrinkage with all sand contents (except zero), but the effect is increased at the higher inclusion areas. This is consistent with our hypothesis, because at the higher sand area fractions, there is less paste initially, so replacing a constant 4% volume fraction of bulk cement paste with air eliminates a greater relative amount of shrinking phase for these microstructures.

B. Three-Dimensional Analytical Result for Dilute Sand Mortars

If the concentration of sand is small enough so each sand grain is relatively unaffected by its neighbors, then the overall shrinkage can be calculated analytically for spherical or ellipsoidal sand grains. The calculated form for this dilute limit for any shape of sand grain is:

$$\frac{\varepsilon^*}{\varepsilon_p} = 1 + \chi c \tag{5}$$

where c is the volume fraction of sand. The factor χ, a dimensionless parameter in three or two dimensions, depends only on the moduli and unrestrained shrinkage ratios between the aggregate, ITZ, and bulk cement paste and on the ratio of the interfacial zone volume (or area) to the sand volume (or area) for a single sand grain and interfacial zone. The derivation of χ for spherical sand grains is given in the Appendix, in both three and two dimensions. To our knowledge, this derivation, though simple, has not been previously published. Figure 6 shows the results of this calculation in three-dimensions for $\varepsilon^*/\varepsilon_p$ plotted versus E_i/E_p for the same values of $\varepsilon_i/\varepsilon_p$ shown in Figure 4, using a volume fraction of $c = 5.9\%$ to match the experimental data discussed later. The qualitative shape of the curves is strikingly similar to the numerical curves shown in Fig-

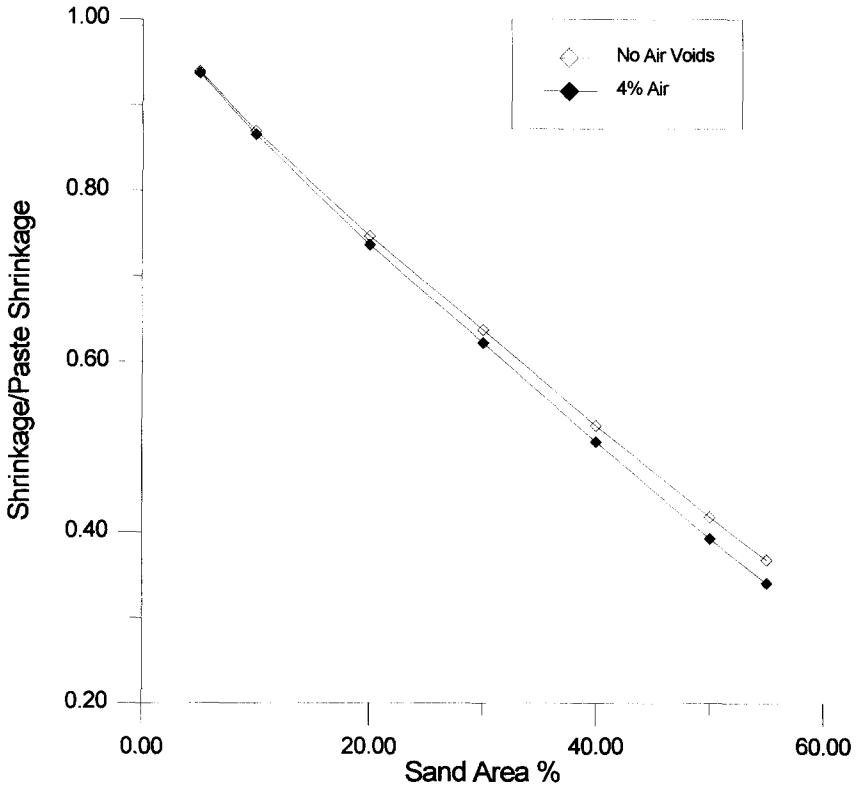

FIGURE 5. Effect of entrapped air on mortar shrinkage for a system of sand particles with diameter 510 μm at varying area coverages. One series contains a constant 4% area coverage of air voids with diameter 110 μm.

ure 4, which tends to justify the overall results generated using the 2-D mortar model for three dimensions. The equivalent calculation for two dimensions in the Appendix also gives qualitatively similar results.

The 3-D analytical result for the shrinkage of dilute sand systems can be used to analyze experiments, if data for such a low sand concentration is available. Such data was measured by Pickett [28] and summarized by Hansen [29]. This data can be used to quantitatively determine the average interfacial zone characteristics, at least for the mortars in Pickett's study [28].

The data set described by Pickett was for a type III portland cement with w/c = 0.35, approximately 65% hydrated, using Ottawa sand. A 5.9% volume fraction of sand is low enough to be considered dilute. A rough size distribution for Ottawa sand was derived from ASTM C778 and is shown in Table 1. The modulus of the aggregate was determined by Hansen [29] to be 4.29 times the bulk paste for Pickett's samples. In this work, the Poisson's ratio of the aggregate is set at 0.2 and the ITZ and paste at 0.3, as with the preceding computations. The value of $\varepsilon^*/\varepsilon_p$ was measured to be 0.93 [28,29]. To fit this value using the 3-D analytical result, the analytical result for χ was averaged over the sand-size distribution shown in Table 1. A variety of combinations of E_i/E_p and $\varepsilon_i/\varepsilon_p$ were tried, with $E_i/E_p < 1$ and $0.2 < \varepsilon_i/\varepsilon_p < 2$. When $0.3 < E_i/E_p < 0.5$, it was found that $0.8 < \varepsilon_i/\varepsilon_p < 1.4$, which seems physically reasonable given the discussion in the previous section. This result implies that intrinsic shrinkage of the interfacial zone cement paste is similar to the bulk cement paste, recalling that the experimental data probably contains inelastic shrinkage, which is not treated in the model at present.

The microstructural origin of this result is not obvious, as the volume fractions of the various phases, shrinking and restraining, are known to change rapidly throughout the interfacial zone. In the next section, results are presented from simulations of cement paste microstructure in the ITZ that help to explain this finding.

IV. Justification of Unrestrained Shrinkage Strain of ITZ

A. Simulation of ITZ Microstructure

To investigate the intrinsic strain of the interfacial zone, the 3-D hydration model developed by Bentz et al. [8] was used to simulate the formation of microstructure in the presence of an aggregate. This model has been used for a variety of studies of the interfacial zone region

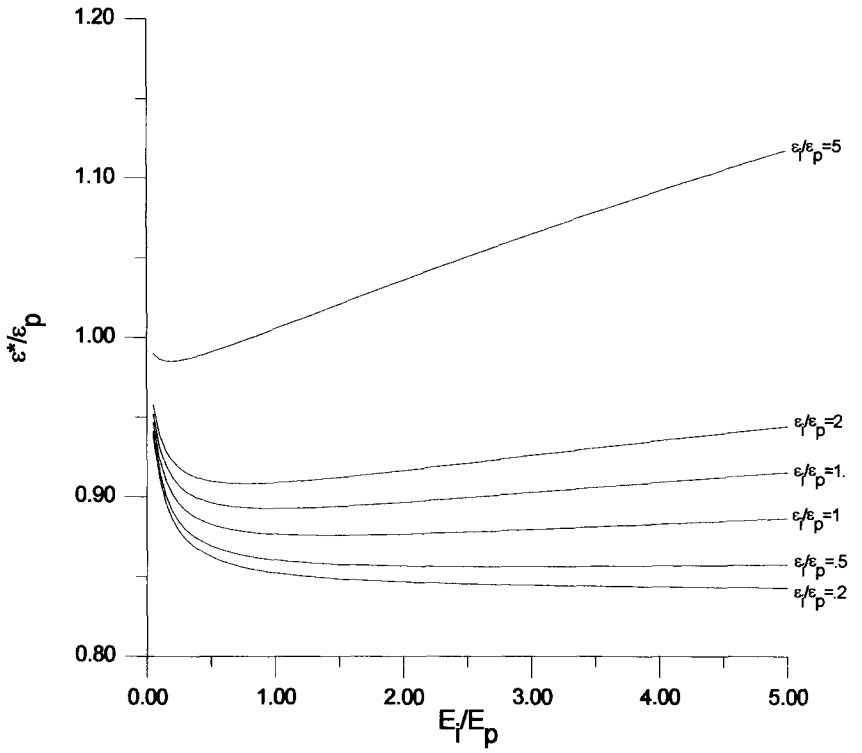

FIGURE 6. Three-dimensional analytical results for overall shrinkage at a sand area fraction of 5.9%.

[11,30–32]. For this particular study, a scale of 1 pixel = 2 μm was used.

Initially, an aggregate 20 μm wide was placed down the middle of a cube measuring 512 × 512 × 512 μm . The width of the aggregate is irrelevant, because only the edge effect on particle packing and one-sided growth effect will have an impact on the development of the interfacial zone [30] in the model.

A particle size distribution for cement was adapted from Coverdale's measurements [33]; the resulting distribution is shown in Table 5. Each particle was placed randomly in the simulation area to avoid overlapping each other or the aggregate.

In the basic hydration model [8], any hydrating tricalcium silicate (C_3S) pixel produces 1.7 pixels of C-S-H and 0.61 pixels of CH. One pixel of the produced C-S-H replaces the hydrating C_3S, and the additional 0.7 pixels of C-S-H and 0.61 pixels of CH are collected and placed randomly within the pore area of the simulation. The result is a more narrow interfacial zone than those recorded experimentally [30].

TABLE 5. Three-dimensional cement particle distribution for simulation of interfacial shrinkage [33]

Diameter (μm)	Volume Percent of Distribution
39	26.5
35	6.0
31	11.25
27	11.25
23	11.25
19	11.25
15	11.25
11	11.25

The simulation described in this paper allowed the additional C-S-H to form only within a cube having an 11-pixel side length, centered on the original position of the dissolving pixel. The goal is to localize the formation of C-S-H and, therefore, widen the resulting interfacial zone to match experiment. CH is still allowed to be placed at random within the pore space. This seems a reasonable assumption given that there is very little silicon in solution, suggesting that the silicon ions probably do not travel far from the cement particle before reacting. However, there is a large amount of calcium in solution [34], requiring a much longer diffusion period before reaction occurs. Additionally, calcium ions (ionic radius = 0.099 nm) [35] will exist individually in the solution (with a small amount of $CaOH^+$), whereas silicon will exist only in the form of much larger ionic species and, thus, will diffuse much more slowly than the individual ions [36].

The simulation was run to approximately 55% hydration. Phase fractions were measured by taking square slices parallel to the surface of the aggregate at every 2 pixels (4 μm) out to a distance of 50 pixels (100 μm)

from the aggregate surface. Slices were then taken every 10 pixels (20 μm). The results are summarized in Figure 7, showing an interfacial zone of about 40 μm in width, a value comparable to those noted by other authors [8,10,36]. The individual phase fractions indicate large gradients within this interfacial zone, as expected.

The porosity has a value of approximately 45% near the aggregate and drops off to a bulk value of 15%. These values are comparable to Scrivener's values (35% at the interface, 7% in the bulk) [10], measured on a 28-day-old specimen, whereas 55% hydration implies a younger and more porous specimen. If the simulated porosity values are inserted into eq 3, the interface/paste modulus ratio is 0.55. Data from a recent study by Bourdette [37] show that the ratio of the interfacial cement paste porosity to the bulk cement paste porosity changes with hydration, assuming a fixed width for the interfacial zone. Thus, the ratio of moduli between interface and bulk will also change with hydration.

The amount of restraining phases in the paste, unreacted C_3S, and CH show a minimum at approximately 20 μm from the surface of the aggregate. This results from the way the CH concentration varies with distance from the aggregate; it starts at a value of 36% near the aggregate and drops to a value of 15% in the bulk, decreasing faster than the amount of unreacted cement increases. The CH concentration is much higher at the interface than anywhere else, due to the completely random placement of newly formed CH in the pore space and the higher volume of pores at the interface than in the bulk paste. These results are supported by experiments that often show elevated CH levels in the interfacial zone [38,39]. The volume fraction of unhydrated cement exhibits an opposing trend, starting at very low values close to the aggregate and increasing to its bulk value farther away from the aggregate. The C-S-H content, on the other hand, exhibits a maximum rather than a minimum at 20 μm, in agreement with recent experimental work by Breton et al. [36].

B. ITZ Shrinkage Simulation

After analyzing the composition of each of the slices, shrinkage analysis in two dimensions was performed, in turn, on each slice. The moduli and intrinsic shrinkage values used are shown in Table 6. The Young's modulus and Poisson's ratio values for C-S-H were extracted from data acquired by Helmuth and Turk [23] for a 24-month-old pure C_3S cement paste with a density of 2.044 g/cc that corresponds roughly to a w/c of .35. The C_3S Young's modulus is that used by Hansen [29]. The moduli for CH was determined by Voigt and Reuss's averaging [40] of the full elastic tensor of CH as determined by Brillouin scattering [41] and agrees well

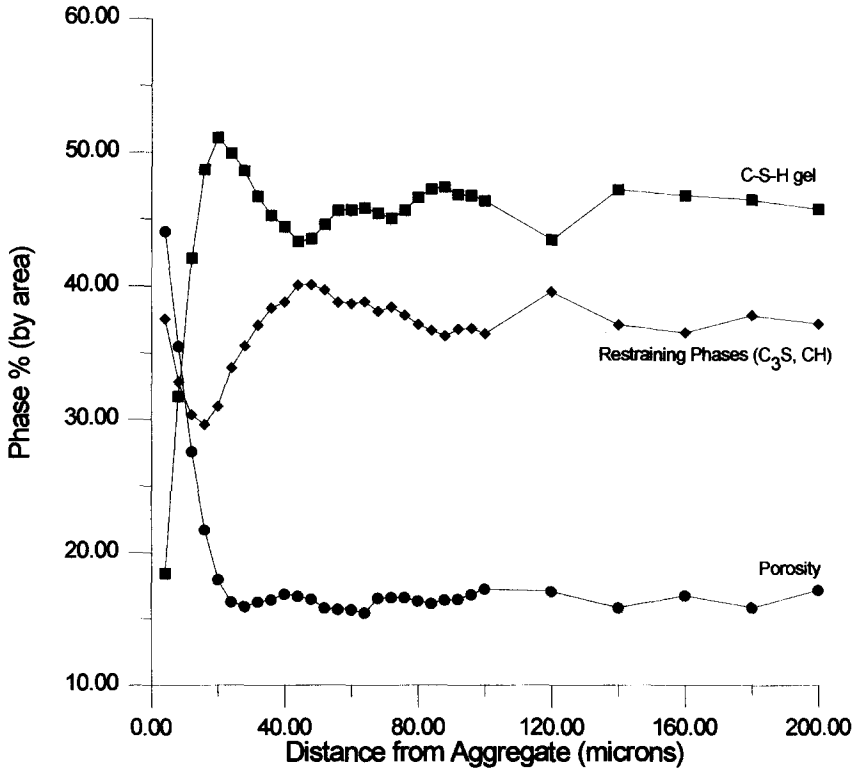

FIGURE 7. Phase volume fraction as determined by the cement paste microstructure model as a function of distance from an aggregate surface.

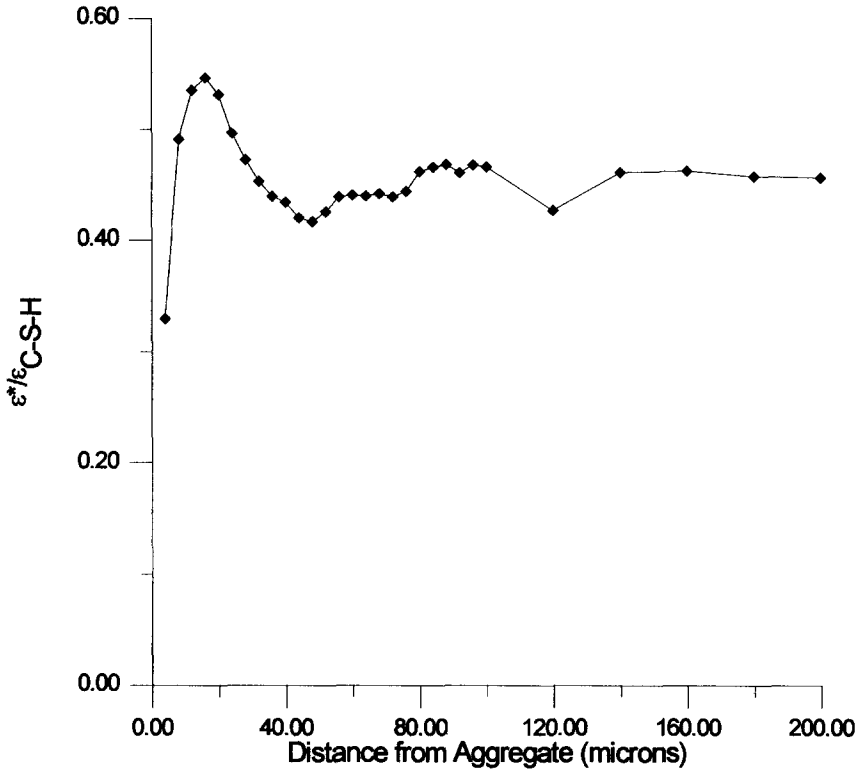

FIGURE 8. Overall shrinkage in the cement paste microstructure model as a function of distance from the aggregate surface.

with experimental data obtained from compressed CH powders [42].

It is noted that computations of shrinkage using 2-D slices of the 3-D interfacial zone microstructure is not the equivalent of a full 3-D shrinkage computation on the entire microstructure, followed by analyzing each slice individually. However, the main value of this method is its feasibility, because we do not yet have a 3-D shrinkage algorithm, and it also serves to focus on each slice, eliminating interactions between different parts of the microstructure at different distances from the aggregate.

The unrestrained strains of the four phases determine the shrinking and nonshrinking phases in the composite. All of the shrinkage is assumed to take place in the C-S-H, while the C_3S and CH are assumed to be nonshrinking. Porosity is also assumed to have no inherent shrinkage, though it may change shape or size as a result of deformation of C-S-H. Since porosity has zero static moduli, the value of its unrestrained shrinkage is irrelevant anyway.

Figure 8 is a graph of computed shrinkage as a function of distance from the aggregate. Comparison with Figure 7 shows a direct correlation between the amount of C-S-H and the amount of shrinkage, as expected. Nevertheless, the most important value is derived from the average value of this region. Examination of Figure 8 shows that the value of bulk shrinkage, obtained far from the interface, coincides closely with the value of the average shrinkage of the interfacial region. This implies that if the ITZ is treated as a shell with uniform properties, as has been done in this paper, the average shrinkage in the ITZ is identical to that of the bulk paste, in accord with the data presented in Section III.

V. Summary

A 2-D finite element shrinkage algorithm has been used to study the effect of structure and properties of the interfacial zone on the elastic moduli and elastic shrinkage of portland cement mortars. Using a combination of 2-D computations and 3-D exact analytical results applied to experimental data for 0.35 w/c cement mortars, it has been shown that the interfacial zone cement paste, when its properties are averaged over a 20-μm thick region, has a Young's modulus of between one third and one half of the bulk cement paste and an intrinsic shrinkage strain that is close to the bulk cement paste. The two major simplifications behind this result are: 1) all shrinkage is elastic and reversible, and 2) the properties of the interfacial zone can be taken as constant, averaged across a 20-μm thick region.

Both 2-D computations and 3-D analytical results show a minimum in shrinkage, as a function of stiffness

TABLE 6. Values used in shrinkage analysis of cement paste microstructure model slices

	Unnormalized			Normalized		
Phase	**E (GPa)**	**υ**	**ε**	***E***	**υ**	**ε**
C-S-H	14	0.27	-1	1	0.27	-1
C_3S	75.9	0.3	0	5.42	0.3	0
CH	43	0.32	0	3.07	0.32	0
pore	0	0	0	0	0	0

in the interfacial zone, for a given unrestrained shrinkage in the ITZ relative to the bulk cement paste. This is directly due to the topology of the interfacial zone, because bulk cement paste can only elastically interact with the aggregate via the interfacial zone and is valid in two and three dimensions. As the interfacial zone becomes very soft, the bulk cement paste essentially decouples from the restraining aggregate, increasing overall shrinkage. On the other hand, as the stiffness of the interfacial zone increases, the coupling becomes stronger, decreasing the magnitude of the overall shrinkage. As the stiffness of the interfacial zone continues to increase, the overall stiffness of the matrix (nonaggregate) phase also increases, enabling it to better resist the nonshrinking aggregate so overall shrinkage starts to increase again. The 2-D computations have also demonstrated that air voids reduce shrinkage by decreasing the modulus of the matrix (nonaggregate) phase and, thus, its ability to resist the nonshrinking aggregate phase.

The quantitative computational accuracy of shrinkage of the nondilute sand mortars is limited by the 2-D nature of the model and the assumption of linear elasticity. However, many of the ideas herein should be applicable in future 3-D simulations. As in the case of electrical properties [14], the 3-D dilute sand limit calculation can be immediately used to extract quantitative information about interfacial zone properties.

Acknowledgments

We wish to thank the Department of Energy for research funding (award No. DE-FGO2-91ER45460/A003). We also gratefully acknowledge the National Science Foundation's Science and Technology Center for Advanced Cement-Based Materials for supporting this work, and R.J. Lee, Inc. for partially funding the development of the 2-D shrinkage finite element algorithm. C.M. Neubauer wishes to thank the National Institute of Standards and Technology for support during an extended visit, during which most of this work was accomplished. Special thanks to Professor A.R. Day for helpful conversations and original contributions regarding development of the finite element code.

Appendix: Exact Shrinkage Calculations for Dilute Sand Content

Analytically solving for the effect of sand grains on the overall shrinkage of the cement paste/sand composite is possible, as far as is known, only in the dilute limit where the volume fraction of sand is small enough to ignore interactions between sand grains. In this limit, which is reasonable for a sand volume fraction of less than about 6–8%, a single inclusion problem can be solved in the following way.

Consider three concentric spheres of radii a, s, and b, with $a < s < b$, with the origin taken at the common center:

$$\begin{aligned} &r < a\text{: phase 3, } K_3, G_3, \varepsilon_3^0 \\ &a < r < s\text{: phase 2, } K_2, G_2, \varepsilon_2^0 \\ &s < r < b\text{: phase 1, } K_1, G_1, \varepsilon_1^0 \end{aligned} \tag{A1}$$

where K_i and G_i are the bulk and shear moduli of the ith phase and ε_i is the isotropic shrinkage strain of the ith phase. Each phase is assumed to be elastically isotropic. The unrestrained shrinkage (eigenstrain) tensor for the ith phase is then:

$$\varepsilon_i^0 = \begin{vmatrix} \varepsilon_{rr} & 0 & 0 \\ 0 & \varepsilon_{\theta\theta} & 0 \\ 0 & 0 & \varepsilon_{\phi\phi} \end{vmatrix} = \begin{vmatrix} \varepsilon_i & 0 & 0 \\ 0 & \varepsilon_i & 0 \\ 0 & 0 & \varepsilon_i \end{vmatrix} \tag{A2}$$

where r, θ, and ϕ are the usual spherical polar coordinates. To make the connection to mortars, phase 3 is designated as sand, phase 2 as interfacial zone cement paste, with $h = s-a<<a$, and phase 1 as bulk cement paste. In the dilute limit $a^3<<b^3$, the volume fraction of sand is small.

In this spherically symmetric problem, only the displacement $u(r)$ is non-zero, where u is the radial component of the elastic displacement vector. Only the radial equilibrium equation then needs to be solved, $\partial\sigma_{rr}/\partial r = 0$. The general solution for u is $u_i(r) = \alpha_i r+\beta_i/r^2$, where $u_i(r)$ is the radial displacement in the i^{th} phase, and α_i and β_i are unknown coefficients that will be determined by the boundary conditions. We note that the unrestrained shrinkage strains of each phase do not come into the equilibrium equation, because they are constants that disappear after the derivative $\partial/\partial r$ is taken. However, they do come into the stress-strain relations, $\sigma_i = C_{ij}(\varepsilon_j - \varepsilon_j^0)$, used to match boundary conditions.

There are five boundary conditions for this problem: σ_{rr} and $u(r)$ are continuous at $r = a$ and $r = s$, and $\sigma_{rr} = 0$ at $r = b$. Once the solution for the displacements are

obtained, the overall shrinkage strain is just $\varepsilon^* = u(r = b)/b$.

The final result is fairly complicated. The composite shrinkage strain, ε^*, *normalized by* ε_1^0, *the unrestrained shrinkage strain of the bulk cement paste matrix (phase 1), is given by*:

$$\frac{\varepsilon^*}{\varepsilon_1^0} = 1 + \chi c_s \tag{A3}$$

where

$$\chi = \frac{\left(1+\frac{V_2}{V_3}\right)\left(K_1+\frac{4}{3}G_1\right)[Y+(K_1+Z)\varepsilon_1^0]}{\varepsilon_1^0 K_1\left(\frac{4}{3}G_1 - Z\right)}$$

and where c_s is the volume fraction of sand, $V_2 = \frac{4}{3}\pi[(a + h)^3 - a^3]$ is the volume of the interfacial zone, $V_3 = \frac{4}{3}\pi a^3$ is the volume of the sand grain, K_1 and G_1 are the bulk cement paste moduli, and

$$Z = \frac{\frac{4}{3}G_2(K_3 - K_2) + \left(1+\frac{V_2}{V_3}\right)K_2\left(K_3+\frac{4}{3}G_2\right)}{(K_3 - K_2) - \left(1+\frac{V_2}{V_3}\right)\left(K_3+\frac{4}{3}G_2\right)} \tag{A4}$$

$$Y = K_2\varepsilon_2^0 - K_1\varepsilon_1^0 + \frac{(K_2\varepsilon_2^0 - K_3\varepsilon_3^0)\left(K_2+\frac{4}{3}G_2\right)}{(K_3 - K_2) - \left(1+\frac{V_2}{V_3}\right)\left(K_3+\frac{4}{3}G_2\right)} \tag{A5}$$

To do the identical problem in two dimensions, simply replace the factor 4/3 in eq A3–A5 by 1, and replace V_2 and V_3 by A_2 and A_3, where A_2 and A_3 are the interfacial zone and sand areas, respectively. This problem has recently been generalized to the case of a gradient of elastic and shrinkage properties surrounding a spherical aggregate [43–45].

References

1. Jennings, H.M.; Xi, Y. In *Creep and Shrinkage of Concrete;* Bazant, Z.P.; Carol, I., Eds.; E&FN Spon: London, 1994; pp 85–102.
2. Garboczi, E.J. *Mater. Struct.* **1993,** *26,* 191–195.
3. Bentz, D.P.; Quenard, D.A.; Baroghel-Bouny, V.; Garboczi, E.J.; Jennings, H.M. *Mater. Struct.* In press.
4. Bentz, D.P.; Garboczi, E.J.; Quenard, D.A. Submitted for publication.
5. Mura, T. *Micromechanics of Defects in Solids, 2nd ed.;* Martinus Nijhoff: Hingham, MA, 1987.
6. Hashin, Z. *J. Appl. Mech.* **1983,** *50,* 481–505.
7. Garboczi, E.J.; Day, A.R. *J. Mech. Phys. Solids* **1995;** *43,* 1349–1362.
8. Bentz, D.P.; Coveney, P.V.; Garboczi, E.J.; Kleyn, M.F.; Stutzman, P.E. *Model. Simul. Mater. Sci. Engin.* **1994,** *2,* 783–808; Bentz, D.P.; Garboczi, E.J. *Guide to Using HYDRA3D: A Three-Dimensional Digital-Image-Based Cement Microstructural Model,* NISTIR 4746; 1992.
9. Eischen, J.W.; Torquato, S. *J. Appl. Phys.* **1993,** *74* (1), 159–170.
10. Scrivener, K.L. In *Materials Science of Concrete I;* Skalny, J.P., Ed.; American Ceramic Society: Westerville OH, 1989; pp 127–161.
11. Bentz, D.P.; Schlangen, E.; Garboczi, E.J. In *Materials Science of Concrete IV;* Skalny, J.P.; Mindess, S. Eds.; American Ceramic Society: Westerville OH, 1995.
12. Winslow, D.N.; Cohen, M.D.; Bentz, D.P.; Snyder, K.A.; Garboczi, E.J. *Cem. Concr. Res.* **1994,** *24,* 25–37.
13. Schlangen, E.; van Mier, J.G.M. In *Material Research Society Symposium Proceedings 278;* Mark, J.E.; Glicksman, M.E.; Marsh, S.P. Eds.; Materials Research Society: Pittsburgh, PA; pp 153–158.
14. Garboczi, E.J.; Bentz, D.P.; Schwartz, L.M. *Adv. Cem. Based Mater.* **1995,** *2,* 169–181.
15. Zimmerman, R.W.; King, M.S.; Monteiro, P.J.M. *Cem. Concr. Res.* **1986,** *16,* 239–245.
16. Hashin, Z.; Shtrikman, S. *J. Mech. Phys. Solids,* **1963,** *11,* 127–140.
17. Thorpe, M.F.; Sen, P.N. *J. Acoust. Soc. Am.* **1985,** *77,* 1674–1680.
18. Snyder, K.A.; Garboczi, E.J.; Day, A.R. *J. Appl. Phys.* **1992,** *72* (12), 5948–5955.
19. Rosen, B.W.; Hashin, Z. *Int. J. Engin. Sci.* **1970,** *8,* 157–173.
20. Nilsen, A.U.; Monteiro, P.J.M. *Cem. Concr. Res.* **1993,** *23,* 147–151.
21. Le Roy, R.; de Larrard, F. *Cem. Concr. Res.* **1994,** *24,* 189–193.
22. Cohen, M.D.; Goldman, A.; Chen, W-F. *Cem. Concr. Res.* **1994,** *24,* 95–98.
23. Helmuth, R.A.; Turk, D.H. *Highw. Res. Board, Spec. Rep.* **1966,** *90,* 135–144.
24. Bentz, D.P.; Garboczi, E.J.; Stutzman, P.E. In *Interfaces in Cementitious Composites;* Maso, J., Ed.; E. & F. Spon: London, 1993; pp 107–116.
25. Mindess, S. In *Materials Science of Concrete I;* Skalny, J.P., Ed.; American Ceramic Society: Westerville, OH, 1989; pp 163–180.
26. Scrivener, K.L.; Gartner, E.M. In *Bonding in Cementitious Composites;* Mindess, S.; Shah, S.P.; Eds.; Materials Research Society: Pittsburgh, PA, 1987; pp 77–85.
27. Rashed, A.I.; Williamson, R.B. *J. Mater. Res.* **1991;** *6,* 2004–2012.
28. Pickett, G. *J. Am. Concr. Inst.* **1956,** *52* (5), 581–590.
29. Hansen, W. *J. Am. Ceram. Soc.* **1987,** *70* (5), 329–332.
30. Garboczi, E.J.; Bentz, D.P. *J. Mater. Res.* **1991,** *6* (1), 196–201.
31. Bentz, D.P.; Stutzman, P.E.; Garboczi, E.J. *Cem. Concr. Res.* **1992,** *22* (5), 891–902.
32. Bentz, D.P.; Garboczi, E.J. *ACI Mater. J.* **1991,** *88* (5), 518–529.
33. Coverdale, R.T. *Ph.D. Dissertation;* Northwestern University; Evanston, IL, 1991.
34. Birchall, J.D.; Howard, A.J.; Bailey, J.E. *Proc. R. Soc. Lond.* **1978,** *A360,* 445–453.

35. Kittel, C. *Introduction to Solid State Physics;* Wiley: New York, 1986; 75.
36. Breton, D.; Carles-Gibergues, A.; Ballivy, G.; Grandet, J. *Cem. Concr. Res.* **1993,** *23,* 335–346.
37. Bourdette, B.; Ringot, E.; Ollivier, J.P. Submitted for publication.
38. Monteiro, P.J.M.; Maso, J.C.; Ollivier, J.P. *Cem. Concr. Res.* **1985,** *15,* 953–958.
39. Detwiler, R.J.; Monteiro, P.J.M.; Wenk, H.R.; Zhong, Z. *Cem. Concr. Res.* **1989,** *18,* 823–829.
40. Watt, J.P.; Peselnick, L. *J. Appl. Phys.* **1980,** *51,* 1525–1531.
41. Holuj, F.; Drozdowski, M.; Czajkowski, M. *Solid State Comm.* **1985,** *56,* 1019–1021.
42. Wittmann, F.H. *Cem. Concr. Res.* **1986,** *16,* 971–972.
43. Garboczi, E.J. Unpublished manuscript.
44. Lutz, M.P.; Monteiro, P.J.M. In *Microstructure of Cement-Based Systems/Bonding and Interfaces in Cementitious Materials,* vol. 370; Diamond, S.; Mindess, S.; Glasser, F.P.; Roberts, L.W.; Skalny, J.P.; Wakeley, L.D.; Eds.; Materials Research Society: Pittsburgh, PA, 1995; pp 413–418.
45. Herve, E.; Zaoui, A. *Int. J. Eng. Sci.* **1993,** *31,* 1–10.